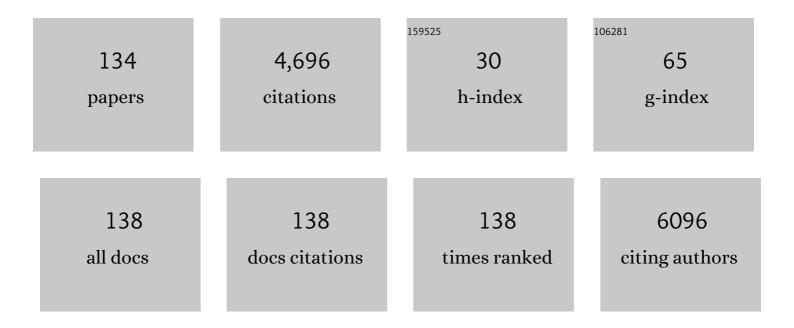
List of Publications by Year in descending order

Source: https://exaly.com/author-pdf/7810204/publications.pdf Version: 2024-02-01



Δριινι Πενλαλι

#	Article	IF	CITATIONS
1	A review of the metastable omega phase in beta titanium alloys: the phase transformation mechanisms and its effect on mechanical properties. International Materials Reviews, 2023, 68, 26-45.	9.4	35
2	Thermal stability and mechanical properties of cold-sprayed Nickel-Yttria coating. Scripta Materialia, 2022, 207, 114281.	2.6	9
3	In-situ radiation response of additively manufactured modified Inconel 718 alloys. Additive Manufacturing, 2022, 51, 102601.	1.7	3
4	An Approach for the Microstructure-Sensitive Simulation of Shear-Induced Deformation and Recrystallization in Al–Si Alloys. Metallurgical and Materials Transactions A: Physical Metallurgy and Materials Science, 2022, 53, 1450.	1.1	0
5	Compositional partitioning during early stages of oxidation of a uranium-molybdenum alloy. Scripta Materialia, 2022, 212, 114528.	2.6	5
6	Decoupling of strain and temperature effects on microstructural evolution during high shear strain deformation. Materialia, 2022, 22, 101402.	1.3	3
7	First-Principles Study of Tritium Trapping in γ-LiAlO ₂ Nanovoids. Journal of Physical Chemistry C, 2022, 126, 5767-5776.	1.5	3
8	Nanotwin assisted reversible formation of low angle grain boundary upon reciprocating shear load. Acta Materialia, 2022, 230, 117850.	3.8	8
9	<i>In-situ</i> observation of deformation twin associated sub-grain boundary formation in copper single crystal under bending. Materials Research Letters, 2022, 10, 488-495.	4.1	5
10	Multi-scale characterization of supersolidus liquid phase sintered H13 tool steel manufactured via binder jet additive manufacturing. Additive Manufacturing, 2022, , 102834.	1.7	4
11	Extended Shear Deformation of the Immiscible Cu–Nb Alloy Resulting in Nanostructuring and Oxygen Ingress with Enhancement in Mechanical Properties. ACS Omega, 2022, 7, 13721-13736.	1.6	3
12	Visualizing the Nanoscale Oxygen and Cation Transport Mechanisms during the Early Stages of Oxidation of Fe–Cr–Ni Alloy Using In Situ Atom Probe Tomography. Advanced Materials Interfaces, 2022, 9, .	1.9	5
13	Metastable orientation relationships in thin film Cu-Cr bilayers. Scripta Materialia, 2021, 194, 113635.	2.6	4
14	Nanostructure and compositional segregation of soft magnetic FeNiâ€based nanocomposites with multiple nanocrystalline phases. Journal of Materials Research, 2021, 36, 105-113.	1.2	6
15	Hydrogen isotopic analysis of nuclear reactor materials using ultrafast laser-induced breakdown spectroscopy. Optics Express, 2021, 29, 4936.	1.7	18
16	Onset of High Methane Combustion Rates over Supported Palladium Catalysts: From Isolated Pd Cations to PdO Nanoparticles. Jacs Au, 2021, 1, 396-408.	3.6	37
17	Phase transformations, microstructural refinement and defect evolution mechanisms in Al-Si alloys under non-hydrostatic diamond anvil cell compression. Materialia, 2021, 15, 101049.	1.3	5
18	Persistence of crystal orientations across sub-micron-scale "super-grains―in self-organized Cu-W nanocomposites. Scripta Materialia, 2021, 194, 113677.	2.6	4

#	Article	IF	CITATIONS
19	Reply to Comment on "A Mechanistic Understanding of Nonclassical Crystal Growth in Hydrothermally Synthesized Sodium Yttrium Fluoride Nanowires― Chemistry of Materials, 2021, 33, 3862-3864.	3.2	1
20	Neutron irradiation induced changes in isotopic abundance of 6Li and 3D nanoscale distribution of tritium in LiAlO2 pellets analyzed by atom probe tomography. Materials Characterization, 2021, 176, 111095.	1.9	15
21	In Situ Atom Probe Tomography Study of The Influence of Deformation on Early Stages of Oxidation of Fe18Cr10Ni Alloy. Microscopy and Microanalysis, 2021, 27, 986-988.	0.2	0
22	Shear-Deformation-Induced Modification of Defect Structures and Hierarchical Microstructures in Miscible and Immiscible Alloys. Microscopy and Microanalysis, 2021, 27, 3106-3108.	0.2	0
23	Development of the Operando Atom Probe: The Influence of the electric field on Fe oxidation. Microscopy and Microanalysis, 2021, 27, 1516-1517.	0.2	0
24	In-situ TEM observation of bending induced sub-grain boundary formation in copper single crystal. Microscopy and Microanalysis, 2021, 27, 3414-3415.	0.2	0
25	3D Nanoscale Analysis of Protein-Mineral Nanoparticle Interfaces Using Atom Probe Tomography for Understanding Amelogenesis. Microscopy and Microanalysis, 2021, 27, 1268-1269.	0.2	1
26	Mechanistic insights into selective oxidation and corrosion of multi-principal element alloys from high resolution and in situ microscopy. Materialia, 2021, 18, 101148.	1.3	6
27	Lattice misorientation evolution and grain refinement in Al-Si alloys under high-strain shear deformation. Materialia, 2021, 18, 101146.	1.3	14
28	The homogenous alternative to biomineralization: Zn- and Mn-rich materials enable sharp organismal "tools―that reduce force requirements. Scientific Reports, 2021, 11, 17481.	1.6	19
29	Molecular-scale investigation of the oxidation behavior of chromia-forming alloys in high-temperature CO2. Npj Materials Degradation, 2021, 5, .	2.6	13
30	Evaluating the microstructure and origin of nonmetallic inclusions in as-cast U-10Mo fuel. Journal of Nuclear Materials, 2021, 554, 152949.	1.3	10
31	Nanomechanical scratching induced local shear deformation and microstructural evolution in single crystal copper. Applied Surface Science, 2021, 562, 150132.	3.1	17
32	Multimodal analysis of spatially heterogeneous microstructural refinement and softening mechanisms in three-pass friction stir processed Al-4Si alloy. Journal of Alloys and Compounds, 2021, 887, 161351.	2.8	9
33	Understanding the microstructural stability in a γ′-strengthened Ni-Fe-Cr-Al-Ti alloy. Journal of Alloys and Compounds, 2021, 886, 161207.	2.8	1
34	Correlating nanoscale secondary ion mass spectrometry and atom probe tomography analysis of uranium enrichment in metallic nuclear fuel. Analyst, The, 2021, 146, 69-74.	1.7	10
35	Detection of hydrogen isotopes in Zircaloy-4 <i>via</i> femtosecond LIBS. Journal of Analytical Atomic Spectrometry, 2021, 36, 1217-1227.	1.6	12
36	Evolution of metastable phases during Mg metal corrosion: An <i>in situ</i> cryogenic x-ray photoelectron spectroscopy study. Journal of Vacuum Science and Technology A: Vacuum, Surfaces and Films, 2021, 39, .	0.9	3

#	Article	IF	CITATIONS
37	Chemical short-range order in derivative Cr–Ta–Ti–V–W high entropy alloys from the first-principles thermodynamic study. Physical Chemistry Chemical Physics, 2020, 22, 23929-23951.	1.3	45
38	New frontiers in atom probe tomography: a review of research enabled by cryo and/or vacuum transfer systems. Materials Today Advances, 2020, 7, 100090.	2.5	34
39	Extreme shear-deformation-induced modification of defect structures and hierarchical microstructure in an Al–Si alloy. Communications Materials, 2020, 1, .	2.9	29
40	Nanoscale Perspectives of Metal Degradation via In Situ Atom Probe Tomography. Topics in Catalysis, 2020, 63, 1606-1622.	1.3	15
41	Rapid assessment of structural and compositional changes during early stages of zirconium alloy oxidation. Npj Materials Degradation, 2020, 4, .	2.6	14
42	Correlating work hardening with co-activation of stacking fault strengthening and transformation in a high entropy alloy using in-situ neutron diffraction. Scientific Reports, 2020, 10, 22263.	1.6	17
43	Carbonaceous deposits on aluminide coatings in tritium-producing assemblies. Nuclear Materials and Energy, 2020, 25, 100797.	0.6	2
44	Precipitation-site competition in duplex stainless steels: Cu clusters vs spinodal decomposition interfaces as nucleation sites during thermal aging. Acta Materialia, 2020, 196, 456-469.	3.8	27
45	A Mechanistic Understanding of Nonclassical Crystal Growth in Hydrothermally Synthesized Sodium Yttrium Fluoride Nanowires. Chemistry of Materials, 2020, 32, 2753-2763.	3.2	27
46	Rapid Response High Temperature Oxygen Sensor Based on Titanium Doped Gallium Oxide. Scientific Reports, 2020, 10, 178.	1.6	28
47	An image-driven machine learning approach to kinetic modeling of a discontinuous precipitation reaction. Materials Characterization, 2020, 166, 110379.	1.9	20
48	Composition-Dependent Microstructure-Property Relationships of Fe and Al Modified Ti-12Cr (wt.%). Jom, 2019, 71, 2321-2330.	0.9	4
49	Direct Observation of Zirconium Alloy Oxidation at the Nanoscale. Microscopy and Microanalysis, 2019, 25, 318-319.	0.2	0
50	Exploring New Science Domains with Atom Probe Tomography Enabled by an Environmental Transfer Hub. Microscopy and Microanalysis, 2019, 25, 276-277.	0.2	1
51	Multimodal Atomic Scale Characterization of Structural and Compositional Changes During Shear Deformation of Materials. Microscopy and Microanalysis, 2019, 25, 2510-2511.	0.2	0
52	Influence of Composition and Structure on Measured H Concentration in beta-Ti Alloys via Atom Probe Tomography. Microscopy and Microanalysis, 2019, 25, 2542-2543.	0.2	0
53	Nanoscale Spatially Resolved Mapping of Uranium Enrichment in Actinide-Bearing Materials. Microscopy and Microanalysis, 2019, 25, 2518-2519.	0.2	1
54	Nanoscale Spatially Resolved Mapping of Uranium Enrichment. Scientific Reports, 2019, 9, 12302.	1.6	16

#	Article	IF	CITATIONS
55	Enhanced Catalyst Durability for Bio-Based Adipic Acid Production by Atomic Layer Deposition. Joule, 2019, 3, 2219-2240.	11.7	12
56	Discontinuous Precipitation in U-10Âwt.%Mo Alloy: Reaction Kinetics, Effect of Prior γ-UMo Microstructure, the Role of Grain-Boundary Misorientation, and the Effect of Ternary Alloying Addition. Jom, 2019, 71, 2770-2779.	0.9	5
57	Injection of oxygen vacancies in the bulk lattice of layered cathodes. Nature Nanotechnology, 2019, 14, 602-608.	15.6	321
58	Crystallographic and compositional analysis of impurity phase U2MoSi2C in UMo alloys. Journal of Nuclear Materials, 2019, 519, 287-291.	1.3	11
59	Outstanding radiation resistance of tungsten-based high-entropy alloys. Science Advances, 2019, 5, eaav2002.	4.7	360
60	Grain boundary segregation and intermetallic precipitation in coarsening resistant nanocrystalline aluminum alloys. Acta Materialia, 2019, 165, 698-708.	3.8	88
61	Multimodal characterization of solution-processed Cu ₃ SbS ₄ absorbers for thin film solar cells. Journal of Materials Chemistry A, 2018, 6, 8682-8692.	5.2	24
62	Onset of phase separation in the double perovskite oxide <mml:math xmlns:mml="http://www.w3.org/1998/Math/MathML"><mml:mrow><mml:msub><mml:mi>La</mml:mi><mml: Physical Review B, 2018, 97, .</mml: </mml:msub></mml:mrow></mml:math 	mn xl2k /mn	nl:nøn>
63	The limiting layer of fish scales: Structure and properties. Acta Biomaterialia, 2018, 67, 319-330.	4.1	53
64	Grain boundary engineering to control the discontinuous precipitation in multicomponent U10Mo alloy. Acta Materialia, 2018, 151, 181-190.	3.8	43
65	Three-dimensional nanoscale characterisation of materials by atom probe tomography. International Materials Reviews, 2018, 63, 68-101.	9.4	119
66	Precipitates and voids in cubic silicon carbide implanted with 25Mg+ ions. Journal of Nuclear Materials, 2018, 498, 321-331.	1.3	7
67	Extraction of rare earth elements using magnetite@MOF composites. Journal of Materials Chemistry A, 2018, 6, 18438-18443.	5.2	30
68	Nanoscale Solute Partitioning and Carbide Precipitation in a Multiphase TRIP Steel Analyzed by Atom Probe Tomography. Jom, 2018, 70, 1752-1757.	0.9	18
69	A Review of Metastable Beta Titanium Alloys. Metals, 2018, 8, 506.	1.0	392
70	Atom Probe Tomography and Correlative Microscopy: 3D Nanoscale Characterization of Metals, Minerals and Materials. Jom, 2018, 70, 1723-1724.	0.9	0
71	Phase transformation of metastable discontinuous precipitation products to equilibrium phases in U10Mo alloys. Scripta Materialia, 2018, 156, 70-74.	2.6	24
72	Study of the radiation damage effect on Titanium metastable beta alloy by high intensity proton beam. Nuclear Materials and Energy, 2018, 15, 169-174.	0.6	15

#	Article	IF	CITATIONS
73	Co-dependent microstructural evolution pathways in metastable δ-ferrite in cast austenitic stainless steels during thermal aging. Journal of Nuclear Materials, 2018, 510, 382-395.	1.3	14
74	Transformation of Active Sites in Fe/SSZ-13 SCR Catalysts during Hydrothermal Aging: A Spectroscopic, Microscopic, and Kinetics Study. ACS Catalysis, 2017, 7, 2458-2470.	5.5	89
75	Radiation Tolerant Interfaces: Influence of Local Stoichiometry at the Misfit Dislocation on Radiation Damage Resistance of Metal/Oxide Interfaces. Advanced Materials Interfaces, 2017, 4, 1700037.	1.9	10
76	Resolving the degradation pathways in high-voltage oxides for high-energy-density lithium-ion batteries; Alternation in chemistry, composition and crystal structures. Nano Energy, 2017, 36, 76-84.	8.2	30
77	Reduced Magnetism in Core–Shell Magnetite@MOF Composites. Nano Letters, 2017, 17, 6968-6973.	4.5	47
78	Kinetics of cellular transformation and competing precipitation mechanisms during sub-eutectoid annealing of U10Mo alloys. Journal of Alloys and Compounds, 2017, 723, 757-771.	2.8	29
79	The natural armors of fish: A comparison of the lamination pattern and structure of scales. Journal of the Mechanical Behavior of Biomedical Materials, 2017, 73, 17-27.	1.5	34
80	Atomic Elemental Tomography of Heavy Element Biomaterials. Microscopy and Microanalysis, 2017, 23, 680-681.	0.2	2
81	Multimodal Imaging of Cation Disorder and Oxygen Deficiency-Mediated Phase Separation in Double Perovskite Oxides. Microscopy and Microanalysis, 2017, 23, 1678-1679.	0.2	1
82	Multimodal and in-situ Chemical Imaging of Critical Surfaces and Interfaces in Advanced Batteries. Journal of Surface Analysis (Online), 2017, 24, 141-150.	0.1	4
83	Laser-material interaction during atom probe tomography of oxides with embedded metal nanoparticles. Journal of Applied Physics, 2016, 120, .	1.1	7
84	Multidimensional Analysis of Nanoscale Phase Separation in Complex Materials Systems. Microscopy and Microanalysis, 2016, 22, 282-283.	0.2	0
85	Exchange bias and bistable magneto-resistance states in amorphous TbFeCo thin films. Applied Physics Letters, 2016, 108, .	1.5	12
86	Stress induced anisotropy in Co-rich magnetic nanocomposites for inductive applications. Journal of Materials Research, 2016, 31, 3089-3107.	1.2	37
87	Competing Pathways for Nucleation of the Double Perovskite Structure in the Epitaxial Synthesis of La ₂ MnNiO ₆ . Chemistry of Materials, 2016, 28, 3814-3822.	3.2	29
88	Pulsed Photothermal Heating of One-Dimensional Nanostructures. Journal of Physical Chemistry C, 2016, 120, 21730-21739.	1.5	3
89	Identifying the Distribution of Al ³⁺ in LiNi _{0.8} Co _{0.15} Al _{0.05} O ₂ . Chemistry of Materials, 2016, 28, 8170-8180.	3.2	77
90	Role of 4- <i>tert</i> -Butylpyridine as a Hole Transport Layer Morphological Controller in Perovskite Solar Cells. Nano Letters, 2016, 16, 5594-5600.	4.5	241

#	Article	IF	CITATIONS
91	Discerning the Location and Nature of Coke Deposition from Surface to Bulk of Spent Zeolite Catalysts. Scientific Reports, 2016, 6, 37586.	1.6	49
92	A low-cost hierarchical nanostructured beta-titanium alloy with high strength. Nature Communications, 2016, 7, 11176.	5.8	213
93	Atomic-scale structural evolution of Ta–Ni–Si amorphous metal thin films. Materials Letters, 2016, 164, 9-14.	1.3	8
94	Role of Calcination Temperature on the Hydrotalcite Derived MgO–Al2O3 in Converting Ethanol to Butanol. Topics in Catalysis, 2016, 59, 46-54.	1.3	64
95	Atom Probe Tomography Characterization of Engineered Oxide Multilayered Structures. Microscopy and Microanalysis, 2015, 21, 845-846.	0.2	0
96	Impact of dynamic specimen shape evolution on the atom probe tomography results of doped epitaxial oxide multilayers: Comparison of experiment and simulation. Applied Physics Letters, 2015, 107, 091601.	1.5	5
97	Effects of crystallographic properties on the ice nucleation properties of volcanic ash particles. Geophysical Research Letters, 2015, 42, 3048-3055.	1.5	18
98	Nanoscale Characterization of Li-ion Battery Cathode Nanoparticles by Atom Probe Tomography Correlated with Transmission Electron Microscopy and Scanning Transmission X-Ray Microscopy. Microscopy and Microanalysis, 2015, 21, 685-686.	0.2	5
99	Level Set Method for Tip Shape Evolution Simulation for Atom Probe Tomography. Microscopy and Microanalysis, 2015, 21, 841-842.	0.2	1
100	Singlet-Oxygen Generation from Individual Semiconducting and Metallic Nanostructures during Near-Infrared Laser Trapping. ACS Photonics, 2015, 2, 559-564.	3.2	14
101	Synergistic effects of iodine and silver ions co-implanted in 6H–SiC. Journal of Nuclear Materials, 2015, 467, 582-587.	1.3	7
102	Simulation of heterogeneous atom probe tip shapes evolution during field evaporation using a level set method and different evaporation models. Computer Physics Communications, 2015, 189, 106-113.	3.0	20
103	Mass Balance and Atom Probe Tomography Characterization of Soft Magnetic (Fe ₆₅ Co ₆₅) _{79.5} B _{13Nanocomposites. IEEE Transactions on Magnetics, 2015, 51, 1-4.}	gt;£i <su< td=""><td>b>2</td></su<>	b>2
104	Visualizing nanoscale 3D compositional fluctuation of lithium in advanced lithium-ion battery cathodes. Nature Communications, 2015, 6, 8014.	5.8	112
105	Conjugated precipitation of twin-related α and Ti2Cu phases in a Ti–25V–3Cu alloy. Acta Materialia, 2015, 84, 457-471.	3.8	32
106	Nanoscale phase separation in epitaxial Cr-Mo and Cr-V alloy thin films studied using atom probe tomography: Comparison of experiments and simulation. Journal of Applied Physics, 2014, 116, .	1.1	10
107	Microstructure of multistage annealed nanocrystalline SmCo2Fe2B alloy with enhanced magnetic properties. Journal of Applied Physics, 2014, 115, .	1.1	16
108	De-vitrification of nanoscale phase-separated amorphous thin films in the immiscible copper–niobium system. Philosophical Magazine, 2014, 94, 1622-1641.	0.7	20

#	Article	IF	CITATIONS
109	Understanding Atom Probe Tomography of Oxide-Supported Metal Nanoparticles by Correlation with Atomic-Resolution Electron Microscopy and Field Evaporation Simulation. Journal of Physical Chemistry Letters, 2014, 5, 1361-1367.	2.1	46
110	Molecular structure and stability of dissolved lithium polysulfide species. Physical Chemistry Chemical Physics, 2014, 16, 10923-10932.	1.3	210
111	Asymmetry of radiation damage properties in Al–Ti nanolayers. Journal of Nuclear Materials, 2014, 445, 261-271.	1.3	8
112	Effects of cooling rate on the microstructure and solute partitioning in near eutectoid Ti–Cu alloys. Philosophical Magazine, 2014, 94, 2350-2371.	0.7	19
113	Subsurface synthesis and characterization of Ag nanoparticles embedded in MgO. Nanotechnology, 2013, 24, 095707.	1.3	23
114	Alpha phase precipitation from phase-separated beta phase in a model Ti–Mo–Al alloy studied by direct coupling of transmission electron microscopy and atom probe tomography. Scripta Materialia, 2013, 69, 513-516.	2.6	36
115	Structure and radiation damage behavior of epitaxial Cr Mo1â^ alloy thin films on MgO. Journal of Nuclear Materials, 2013, 437, 55-61.	1.3	6
116	Structure analysis of a precipitate phase in an Ni-rich high-temperature NiTiHf shape memory alloy. Acta Materialia, 2013, 61, 3335-3346.	3.8	138
117	Role of Photoexcitation and Field Ionization in the Measurement of Accurate Oxide Stoichiometry by Laser-Assisted Atom Probe Tomography. Journal of Physical Chemistry Letters, 2013, 4, 993-998.	2.1	121
118	Laser assisted crystallization of ferromagnetic amorphous ribbons: A multimodal characterization and thermal model study. Journal of Applied Physics, 2013, 114, .	1.1	25
119	Composition Analysis on the Precipitates in the NiTiHf and NiPdTiHf Alloys. Microscopy and Microanalysis, 2013, 19, 1518-1519.	0.2	1
120	Coupling Atom Probe Tomography with Aberration-Corrected Scanning Transmission Electron Microscopy and First-Principles Computations to Investigate Omega Precipitation in Titanium Alloys. Microscopy and Microanalysis, 2013, 19, 946-947.	0.2	0
121	Compositional and Chemical Segregation in Li1.2Ni0.2Mn0.6O2 Cathode Materials Characterized by Atom Probe Tomography and Scanning Transmission X-ray Microscopy. Microscopy and Microanalysis, 2013, 19, 964-965.	0.2	1
122	A Level Set Evaporation Model for Heterogeneous Atom Probe Tip. Microscopy and Microanalysis, 2013, 19, 934-935.	0.2	0
123	Characterization of embedded metallic nanoparticles in oxides by cross-coupling aberration-corrected STEM and Atom Probe Tomography. Microscopy and Microanalysis, 2012, 18, 912-913.	0.2	3
124	Controlling axial p-n heterojunction abruptness through catalyst alloying in vapor-liquid-solid grown semiconductor nanowires. Microscopy and Microanalysis, 2012, 18, 1860-1861.	0.2	0
125	Non-classical homogeneous precipitation mediated by compositional fluctuations in titanium alloys. Acta Materialia, 2012, 60, 6247-6256.	3.8	129
126	Experimental evidence of concurrent compositional and structural instabilities leading to ω precipitation in titanium–molybdenum alloys. Acta Materialia, 2012, 60, 596-609.	3.8	248

#	Article	IF	CITATIONS
127	Competing Martensitic, Bainitic, and Pearlitic Transformations in a Hypoeutectoid Ti-5Cu Alloy. Metallurgical and Materials Transactions A: Physical Metallurgy and Materials Science, 2011, 42, 1139-1143.	1.1	20
128	Phase separation and formation of omega phase in the beta matrix of a Ti–V–Cu alloy. Acta Materialia, 2011, 59, 2981-2991.	3.8	72
129	Novel Mixed-Mode Phase Transition Involving a Composition-Dependent Displacive Component. Physical Review Letters, 2011, 106, 245701.	2.9	113
130	Three-dimensional morphology and composition of omega precipitates in a binary titanium–molybdenum alloy. Scripta Materialia, 2009, 61, 701-704.	2.6	78
131	Phase separation in immiscible silver–copper alloy thin films. Journal of Materials Science, 2009, 44, 3393-3401.	1.7	28
132	Investigations of Omega Precipitation in Titanium Molybdenum Alloys by Coupling 3D Atom Probe Tomography and High Resolution (S)TEM. Microscopy and Microanalysis, 2009, 15, 268-269.	0.2	5
133	Combined Synchrotron X-Ray Diffraction and Digital Image Correlation Technique for Measurement of Austenite Transformation with Strain in TRIP-Assisted Steels. , 0, , .		7
134	Phase Transformations, Microstructural Refinement and Defect Evolution Mechanisms in Al-Si Alloys Under Non-Hydrostatic Diamond Anvil Cell Compression. SSRN Electronic Journal, 0, , .	0.4	0